Arabian Journal for Science and Engineering (2023) 48:16431–16443
https://doi.org/10.1007/s13369-023-08325-3

RESEARCH ARTICLE-CHEMICAL ENGINEERING

La-doped TiO_2 Nanoparticles for Photocatalysis: Synthesis, Activity in Terms of Degradation of Methylene Blue Dye and Regeneration of Used Nanoparticles

Veeresh Verma[1] · Satya Vir Singh[1]

Received: 3 March 2023 / Accepted: 19 September 2023 / Published online: 13 October 2023

Abstract
In this study, bare and Lanthanum (La)-doped TiO_2 photocatalysts $Ti_{1-x}La_xO_2$ ($x = 0.00$–0.025) were prepared by employing a solution-combustion procedure. In this, citric acid was utilized as fuel and as a complexing agent. The prepared photocatalysts were characterized by FTIR, FE-SEM, XRD, DRS and XPS. The XRD confirms that prepared TiO_2 photocatalysts have only the anatase phase, and also, crystallite size was calculated which is 30.16 and 19.90 nm for bare and $Ti_{0.985}La_{0.015}O_2$, respectively. The DRS shows that with increasing the doping concentration of La in TiO_2, a continuous shifting in absorbance towards the visible light region was observed. The FTIR determines the O–H band, Ti–O–La, and several other functional groups present in the synthesized bare and La-doped TiO_2 photocatalysts. The XPS spectra confirm the existence of all expected elements (Ti, O, and La) in the synthesized photocatalysts. The FE-SEM confirms spherical shape of prepared photocatalysts, and particle size of bare and $Ti_{0.985}La_{0.015}O_2$ was 32.28 and 22.24 nm, respectively, which agrees with XRD data. Photocatalytic breakdown of methylene blue (MB) dye in its aqueous solutions of different concentrations (10, 20, 30, 40 and 50 ppm) was found to be first order. The best activity was shown by $Ti_{0.985}La_{0.015}O_2$, and it was better than the commercial aeroxide P-25 photocatalyst. The $Ti_{0.985}La_{0.015}O_2$ catalyst could be regenerated and reused up to five times with a minor loss in degradation efficiency of MB dye (30 ppm) about 7.85% at the end of fifth cycle, however, with fresh catalyst degradation was 88.71% .

Keywords Photocatalysis · Lanthanum doping · Solution-combustion · Regeneration · Methylene blue dye

1 Introduction

Various water contaminants, primarily dyes, occur due to recent industrial development and improvement in standard of living. The organic dyes are frequently used to produce textiles, leather and papers, generating loads of water pollution [1]. Among various dyes used in these industries, methylene blue (MB) is an organic dye that is toxic; non-biodegradable; environmentally persistent and stable to light, water, heat and oxidation. MB dye is a widely utilized basic and cationic dye with an array of applications. However, when discharged into water bodies, MB poses a significant threat to aquatic animals' life. Exposure to MB can cause detrimental effects such as a rapid heartbeat, nausea, vomiting, shock, cyanosis, jaundice, and tissue necrosis. It also causes Heinz bodies, cyanosis, jaundice, quadriplegia, and tissue necrosis in humans. These negative effects highlight the significance of preventing the release of MB into waterways to protect the health of ecosystems and human populations [2–4]. To accomplish the rising exigency for water in various industries and for agriculture, wastewater should be cleaned for reuse. Because of their high durability and aromatic behaviour, biological and physical treatments typically fail to remove dyes from wastewater efficiently [5]. For instance, water-borne microbes cannot break dyes and yield several toxic substances during decomposition. Additionally, physical methods like reverse osmosis [6], ultrafiltration [7] and activated carbon adsorption [8] can transport organic molecules to alternative phases that can result in next-generation contaminants. These contaminants require post-treatment, which adds to the expense [9, 10]. They also result in the problem of management of solid waste.

✉ Satya Vir Singh
svsingh.che@itbhu.ac.in

[1] Department of Chemical Engineering and Technology, IIT (BHU), Varanasi, Uttar Pradesh 221005, India

New methods for wastewater treatment are constantly being established to completely degrade toxins without negatively impacting the atmosphere or human health. Advanced oxidation processes (AOPs) have been considered for usage in wastewater purification in recent decades, aiming to complete mineralization of pollutants into harmless end products [11]. Various AOPs such as vacuum-UV (VUV) photolysis, photocatalytic oxidation, UV/O_3, UV/H_2O_2 and fenton-like processes are used [12]. To eliminate various forms of organic and inorganic pollutants from aqueous solutions non-selectively, AOPs utilize hydroxyl free radicals (·OH) and reactive oxygen species, which, once produced, are highly effective and intensely oxidizing species. AOP is preferred over other methods because they are environment friendly as they neither transfer pollutants from one phase to another nor they produce hazardous sludge upon treatment of pollutants [13].

Solar photocatalysis using TiO_2 semiconductor is one of the AOP techniques used to produce ·OH free radicals. The ability to use radiation from the sun to stimulate the photocatalyst is another advantage of this technology. In that situation, the cost of the treatment would be far lower than the cost of using artificial radiation, and it might be more readily applied in the industry [14, 15]. Because of its beneficial properties, non-toxicity, low cost, chemical stability, and environmental sensitivity, titanium dioxide (TiO_2) has been accepted as an inherent semiconductor material for the breakdown of hazardous organic compounds in aqueous solution [16].

The most popular photocatalyst for air purification and wastewater treatment is TiO_2. However, because photogenerated pairs of electron and hole recombine quickly, the photocatalytic degradation efficiency is still relatively low. So, a current key obstacle in this field is enhancing photocatalytic efficiency. It has been demonstrated that doping in the lattice of TiO_2 is an efficient way to surge the activity of photocatalysis [17]. Rare earth ion doping surges considerably the photocatalytic performance of TiO_2, and by capturing photogenerated electrons, it can also improve the efficiency of electron–hole pair separation [18–23].

Pairs of electron and hole are generated when a semiconductor, such as TiO_2, is subjected to light quanta with energies higher than that of the band gap. These photoexcited species (e^+/h^+) can diffuse on the surface of photocatalyst and interact with molecules that have been adsorbed in redox processes. The principal reactions are the oxidation of water molecules or OH^- by holes to create ·OH free radicals because water molecules outweigh contaminant molecules. The superoxide radical ($\cdot O_2^-$), a lesser reactive species of oxygen than the radical ·OH, which can strike the organic substances or, through various events, ultimately release the ·OH free radical, is also produced when a photogenerated electron reacts with adsorbed oxygen and this ·OH free radical breaks organic substances [24, 25].

Unfortunately, TiO_2's industrial utilization is constrained by its broad band gap values and fast recombination rate of photogenerated pairs of hole and electron [26]. Metal ions such as Cu, Fe, Mn, and Co [27–29] and non-metal ions such as S, N, C, F, I and B [30–33] doping are used to improve the characteristics of TiO_2. Researchers' attention is now focused on rare earth elements, i.e. Er, La, Eu and Y-doped titanium dioxide. La-doped compounds are commonly utilized as competent catalysts resulting from 4*f* electron transition.

Rutile-anatase transition in TiO_2 doped with La is radius dependent. The large atomic radius has a more significant inhibitory effect on anatase–rutile TiO_2 transformation [34].

Recent publications have revealed that doping rare earth elements reduce band gap values of TiO_2 [34, 35]. This sparked the idea of doping TiO_2 with La to create an effective photocatalyst. In present work, La has been doped in TiO_2 to reduce the band gap so that visible light may be used for photocatalysis. Also, La doping promotes the separation of electrons and holes and reduces rate of recombination of the charge carrier and hence, La doping improves TiO_2 photo reactivity.

As far as we know, this paper covers the synthesis of TiO_2 doped with La using inexpensive TiO_2 powder by straightforward citric acid-assisted solution-combustion procedure and annealing to increase the crystallinity of the nanoparticles. The conditions under which the particles were produced significantly impacted their size and form. The activity of nanoparticles as photocatalyst was determined by kinetics photodegradation of MB dye.

2 Materials and Methods

2.1 Chemicals Used

The chemicals employed in the preparation of TiO_2 nanoparticles are as follows. TiO_2 powder with a purity of 99%, ammonia sulphate GR [$(NH_4)_2SO_4$], sulfuric acid (H_2SO_4) 98%, liquor ammonia sp. gr. is 0.91 (about 30% NH_3), lanthanum nitrate with a purity of 99%, citric acid monohydrate GR ($C_6H_8O_7H_2O$), MB dye and Nitric acid GR (HNO_3). All of the above chemicals were acquired from Merck, India.

2.2 Synthesis of Doped TiO_2 Nanoparticles

The doped TiO_2 crystalline nanoparticles were synthesized by solution-combustion process from TiO_2 powder in a similar manner as reported earlier [27, 33, 36, 37]. The process is described for 1 mol % La doping. The 4.7289 g of TiO_2 was dissolved in 100 mL of sulphuric acid, and six times mol of TiO_2 ammonium sulphate was added. The resulting solution was heated with the hot plate using a magnetic bead at about

400 rpm for 2–3 h at a temperature of 180 °C, which resulted in titaniumoxysulphate, $TiO(SO_4)$. In another beaker, lanthanum nitrate (0.000626 mol) was added to 50 mL sulfuric acid for 1% La doping, and for other La doping, the $La(NO_3)_3$ amount was added according to stoichiometry. The hot plate was used to heat the resulting dispersions with the help of magnetic stirrer at about 300 rpm for 2–3 h at 170 °C. Then, both solutions were mixed hot and cooled to ambient and using distilled water made up to 500 mL of total volume.

Then, ammonia (NH_3) solution was added gradually so that a white residue was obtained, which was separated through the Buchner funnel. This residue was mixed with 100 mL of HNO_3 to form titanium oxynitrate, $TiO(NO_3)_2$. About 10 g of complexing agent, i.e. monohydrate citric acid, was added, and the total solution was made up to 500 mL by adding double-distilled water. After that, the entire contents were evaporated over a hot plate at 70–80 °C with steady stirring till self-ignition occurred. Ignition took place in an open atmosphere at ambient temperature, and burning occurred by self-promulgating combustion, evacuating significant gases and forming a fluffy brown mass of La-doped TiO_2 that was crushed into powder with a pestle and mortar. Citric acid is utilized as a complexing agent, forming a complex with cations and acting as fuel for the combustion process in the ignition step. The temperature was uplifted by the ignition stage, which resulted in the formation of crystalline powder at a low temperature. The powdered La-doped TiO_2 product was calcined in the presence of the air for 5 h at 500 °C. This resulted in the final TiO_2 nanoparticles doped with La.

2.3 Characterisations

Employing XRD analysis with Cu-K irradiation (Rigaku Ultima IV, Japan), the average particle size and phase of the obtained undoped and La-doped TiO_2 (with 0.005, 0.01, 0.015, 0.02, and 0.025%) nanoparticles were examined. When determining the band gap energies of the synthesized photocatalysts, the Kubelka–Munk method was used to analyse the data from the DRS analysis (CORY 100 Bio UV spectrophotometer) using barium sulphate as the reference. The Nicolet 5700 (Thermo Electron) FTIR spectrophotometer was used to record the infrared spectra using the KBr pellet method. Using monochromated Mg–K (1253.6 eV) as the X-ray source (AMICUS, Kratos Analytical, England), the XPS analysis was performed to determine the chemical state and binding energy of elements contained in the produced photocatalysts. XPSPEAK41 and ImageJ software were used to analyse XPS and FESEM data, respectively. All the graphs were plotted using Origin 2019b software.

2.4 Photocatalytic Reactor for the Degradation of Dye Solution

The synthesized $Ti_{1-x}La_xO_2$ ($x = 0.00$, 0.005, 0.01, 0.015, 0.02 and 0.025) nanoparticles were used to photodegrade the MB dye in UV photochemical reactor (UV-PCR).

The UV-PCR (Fig. 1) is fortified with 8W UV tubes (Philips TUV 8W G8T5 Hg) and a stirrer obtained from Perfit India Limited, Ambala, India. Dye solutions were treated in a quartz tube throughout. Only 100 mL of dye solution and nanoparticles was treated so that it properly mixed during the photolysis reaction. The 100 mL of the MB solution was taken without any photocatalyst and put in UV-PCR and exposed to UV light for 3 h to assess the self-degradation of dye. A 2 mL sample was tested for dye concentration every 10 min during the process.

The dye is also adsorbed on the surface of the photocatalyst. Adsorption studies were therefore performed to know the affinity of dyes for the photocatalysts. 100 mL solution of the dye was placed in the tube, and 0.01 g of the photocatalyst was mixed to it to investigate and the dye adsorption by photocatalysts. The tube was covered with black foil to prevent photocatalysis by ambient visible light. The tube was maintained for 1 h with constant agitation in UV-PCR, and its lights were not made on. 2 mL of dye solution was drawn from the tube after every 10 min and centrifuged, and dye concentration was determined.

The experimental methods described above were used throughout. The photocatalyst $Ti_{0.985}La_{0.015}O_2$ exhibited the highest photocatalytic activity amid all prepared photocatalysts and was therefore used in this study to measure the activity of photocatalysis.

By deducting the decrease in dye concentration because of adsorption on photocatalyst and the deficit of dye due to autolysis in solution, the true decrease in dye in simulated solution of dye because of photodegradation by the photocatalyst was estimated. The photocatalytic degradation of MB dye in the simulated dye solution was calculated by the formula: [33]

$$\text{Change of concentration by photo degradation} = (C_a - C_b) - C_c - C_d \quad (1)$$

where C_a and C_b are initial and ultimate concentrations in the dye solution, respectively. C_c and C_d represent the reduction in concentration due to dye adsorption and dye reduction in the final solution.

2.5 Reusability of Used Photocatalyst

The performance of used 1.5% La-doped TiO_2 photocatalyst for degradation of aqueous MB dye was explored after

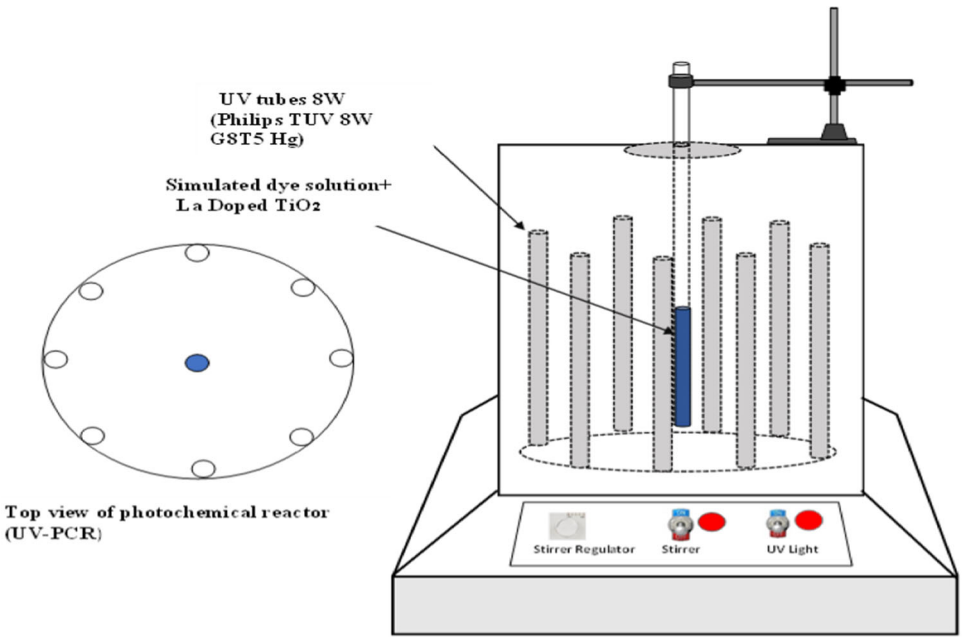

Fig. 1 Graphical representation of UV-photochemical reactor

regeneration. The regeneration was done five times after each use. The photocatalyst was regenerated using the following method. To separate the photocatalyst loaded with dye from the overall solution, the entire mixture of photocatalyst and photodegraded dye was centrifuged at 3000 rpm for 20 min and the photocatalyst was deposited at the bottom and separated. With this double-distilled water was added and again centrifuged for 20 min at 3000 rpm and a photocatalyst loaded with dye was separated at bottom. This photocatalyst slurry was put into a glass petri dish, and its water was evaporated in a drier at 102 °C. The dye-loaded, La-doped nanoparticles were taken out and put in the crucible to undergo a five-hour calcination process at 500 °C to get a regenerated catalyst, ready for use.

2.6 Methodology of Kinetic Study

100 mL of the dye solution was introduced into quartz tube of the UV-PCR for dye degradation kinetics analysis, and 0.01 g of prepared nanoparticles was added to this tube. After inserting magnetic bead, the tube was put inside the UV-PCR to allow the dye to be photodegraded. The dye starts to photodegrade as soon as the UV PCR lamp was switched on. Constant stirring was used to comprehensively mix the dye solution and photocatalyst during the photocatalytic process. A 2 mL sample was collected from the tube after every 5 min and centrifuged for 2 min before measuring its concentration. The same procedure was used with all catalysts. The different catalysts prepared with La doping (0, 0.5, 1, 1.5, 2.0 and 2.5%) were used, and dye concentrations in solution were 10, 20, 30, 40 and 50 ppm. For comparison of catalysts, the kinetic studies with commercial TiO_2 nanoparticles aeroxide P-25 (bought from Sigma-Aldrich) were also carried out.

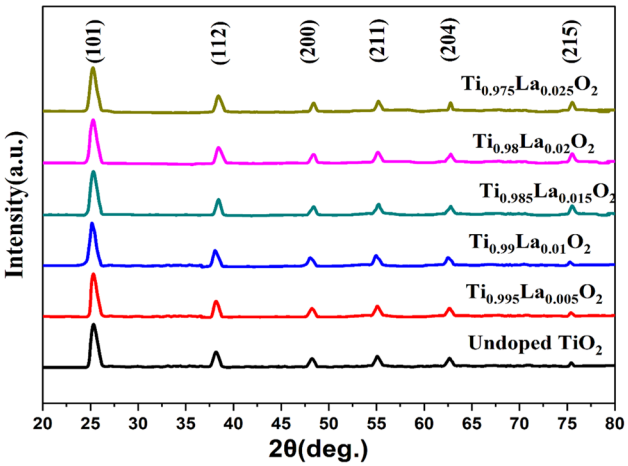

Fig. 2 XRD diagram of La-doped and undoped TiO_2 photocatalysts

3 Results and Discussion

3.1 XRD

X-ray diffraction was used to understand the consequence of various percentages of La doping in TiO_2 and investigate the crystal structure. In Fig. 2, XRD plots for undoped TiO_2 and doped TiO_2 have been shown. All the prepared nanoparticles have anatase phase without any significant rutile phase [38].

Figure 2 also shows that doping of La within TiO_2 does not same as bare TiO_2. The peak at the 2θ (25.351) corresponds to plane alter the structure of TiO_2 as it remains 101 of anatase phase. Meanwhile, Lanthanum ionic radius has the value of 1.03 Å which is greater than that of Titanium, which has a value of 0.62 Å, so it cannot replace the Ti ion and leftovers at interstitials of Titanium dioxide beneath the range of scan of XRD. So, these dissimilarities between La and Ti ions radii may create bonds of Ti–O–La or lanthanum oxide (La_2O_3) at the anatase surface relative to actual assimilation of La^{3+} in the lattice of the TiO_2. The La_2O_3 peak is not present in the XRD plot because it is scattered and cannot be discovered in the XRD pattern [35]. It is also evident from Fig. 2 that on increasing doping percentage of La, the intensities of prepared samples also increase significantly. With a rising La percentage of doped nanoparticles, notably for anatase phase, values of crystallite size of synthesized La-doped TiO_2 samples significantly diminish and recombine capacity of pairs of electron–hole on excitation of La^{3+} on TiO_2 is inhibited, promoting the activity of photocatalysis of prepared photocatalysts [39].

The crystallite size was calculated using Debye Scherer's equation [40].

$$d = 0.9\lambda/\beta \mathrm{Cos}\theta \tag{2}$$

where d is crystallite size, β is full width at half maximum, λ is radiation wavelength (1.5406 Å), and θ is the angle of diffraction.

The average crystallite size of TiO_2 and 1.5% La-doped TiO_2 was found to be 30.16 and 19.90 nm, respectively. A similar result would also be found by Zhan et al. [41].

3.2 FTIR

Fourier transform infrared spectroscopy was applied to detect distinct functional groups in the lanthanum-doped and undoped TiO_2 photocatalysts. The FTIR spectra presented in Fig. 3 show the stretching vibrations of OH functional group at the wavenumber of 3450 cm^{-1}. All the La-doped and undoped photocatalysts peak at the wavenumber of 1020 cm^{-1}, which relates to the anatase phase of Ti–O vibrations. Undoped TiO_2 shows a band at the wavenumber of 512 cm^{-1}, a characteristic peak of TiO_2, but with doped TiO_2 with La, this characteristic peak shifts at 480 cm^{-1}, which might correspond to bond structure of Ti–O–La. Sibu et al. [42] also reported these results in a similar range. The band spectra situated at the wavenumber of 1620 cm^{-1} validate the occurrence of OH groups at photocatalysts' surface, also called bending vibrations of the water (H–O–H bending) molecules which are absorbed at the surface of nanoparticles. Nie et al. [43] and Coromelci et al. [44] also reported occurrence of OH group and vibrations of water molecules in similar range.

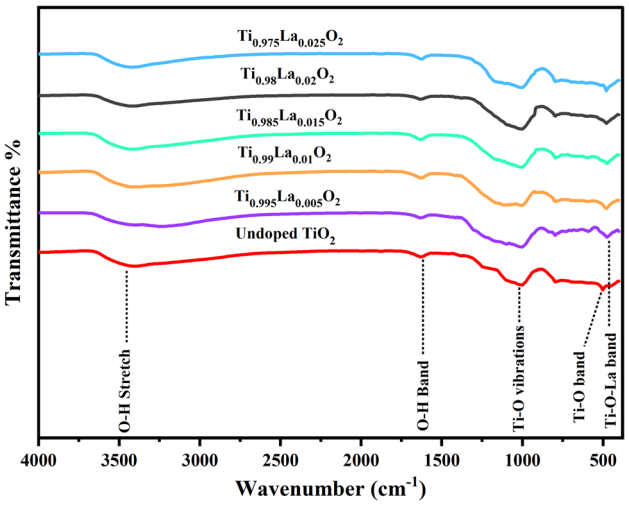

Fig. 3 FTIR plots of La-doped and undoped TiO_2 photocatalysts

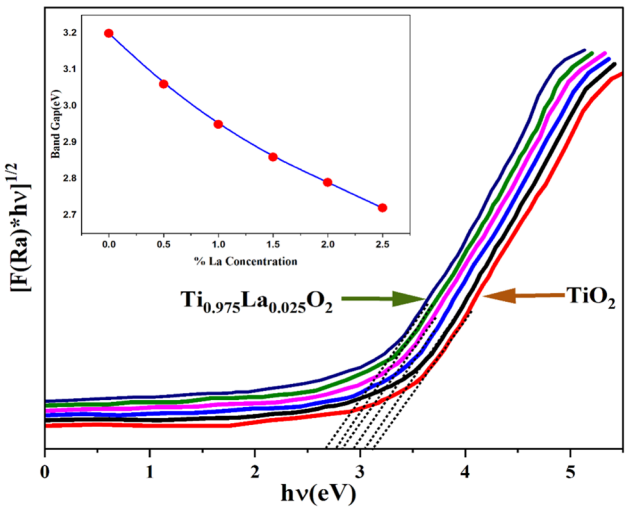

Fig. 4 DRS plots of La-doped and undoped TiO_2 photocatalyst

3.3 DRS

The optical absorbance spectra of synthesized TiO_2 doped with La and bare TiO_2 were measured in the UV–visible range and are presented in Fig. 4. The indirect band gap of bare TiO_2 and doped with La was calculated with the help of the plots of $[F(R\alpha)*h\upsilon]^{1/2}$ versus $h\upsilon$ (Fig. 4), where $F(R\alpha)$ is called the Kubelka–Munk function and may be represented as:

$$F(R\alpha) = (1 - R\alpha)^2/2R\alpha \tag{3}$$

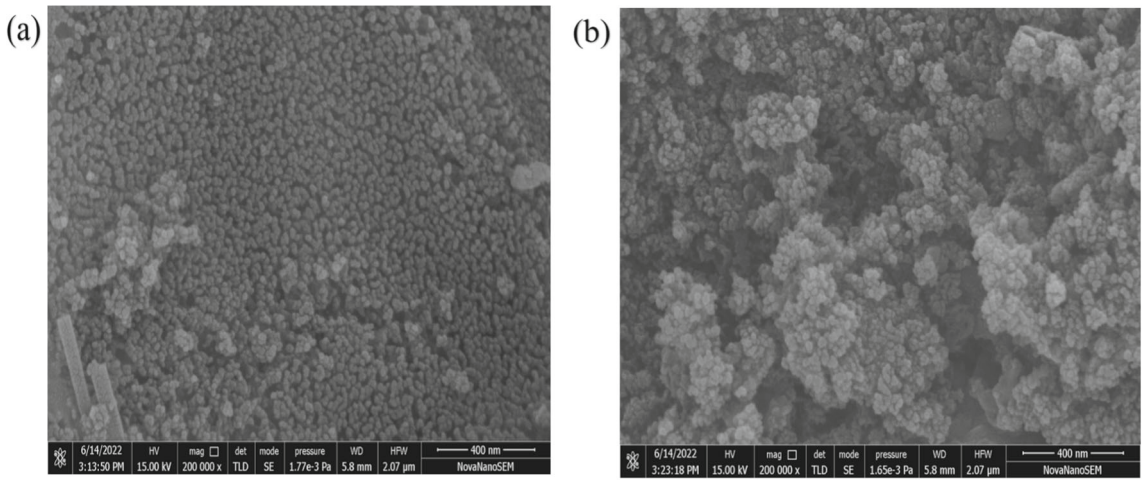

Fig. 5 FE-SEM Pictures of **a** undoped **b** 1.5% La-doped TiO_2 photocatalysts

where $R\alpha = 10^{-A}$ is the reflectance coefficient of catalyst determined from absorbance data.

It is noticeable from inset of Fig. 4 that band gap values of prepared nanoparticles are decreased from 3.2 to 2.7 eV on rising doping percentages of lanthanum from 0 to 2.5%. Nie et al. [43] also reported a decrease in band gap values on increasing La doping in TiO_2 photocatalysts.

Results show that metals addition into TiO_2 photocatalysts causes a slight reduction in band gap values. This variation in band gap values may be the result of the dielectric confinement effect. The occurrence of this type of band corresponds to the displacement of charge to conduction band from valence band of TiO_2 (because of 2*p* orbital of oxygen). Due to the fact that the dielectric constant of La_2O_3 is lower than that of TiO_2, the energy change brought on by dielectric confinement (due to doping of La) is more significant than that brought on by the impact of space limitations on electron holes and which is evident from the decrease in band gap values is therefore detected that is known as red-shift [45].

3.4 FE-SEM

FE-SEM was used to conduct the morphological and microstructural analysis of the prepared bare and La-doped photocatalysts. In Fig. 5, FE-SEM images of the prepared photocatalysts bare and 1.5% La-doped TiO_2 are shown. From these pictures, it is evident that photocatalysts are of spherical shape. It is also clear from these figures that the morphology of doped photocatalysts remains unchanged, and some agglomeration may be due to the magneto-dipole interaction. It is also accomplished that doped photocatalysts' particle size is decreased compared to undoped one, having sizes approximately 22.24 and 32.28 nm, respectively. It agrees with the XRD data. This is beneficial because when size of the particle is decreased, surface area is increased, which enhances photocatalytic sites, which eventually increases photocatalytic activity of prepared samples [45–47].

3.5 XPS

The XPS was applied to analyse the composition of elements present at the surface and the chemical oxidation state of nanoparticles [48]. Figure 6a represents the full scan spectra which confirms the presence of O and Ti elements on the bare TiO_2's surface and presence of O, Ti and La on 1.5%-doped TiO_2's surface.

In Fig. 6b, XPS spectra of 2*p* orbital of Ti are represented in bare TiO_2 and 1.5% La-doped TiO_2. Both doped and undoped samples show two noticeable peaks attributed to Ti $2p_{3/2}$ and Ti $2p_{1/2}$, respectively, indicating that the normal tetravalent oxidation state of titanium predominates Ti^{4+} in anatase TiO_2 [49]. The binding energy of undoped TiO_2 sample is 458.6 and 464.4 eV. After doping of La 1.5% binding energy increases by 0.2 eV and peaks shifts to higher values which shows the existence of various electronic interactions amid Ti and oxides of La because of their difference in electronegativity, which lowers Titanium external electron density and therefore, raises Ti 2*p*'s binding energy [50].

In Fig. 6c, XPS plot of undoped TiO_2 for O 1*s* is shown. The peaks at binding energy of 529.3 eV and 531.1 eV are accredited to lattice oxygen and OH group, respectively, in undoped TiO_2 samples. In Fig. 6d, XPS plot for 1.5% La-doped TiO_2 has been shown for O 1*s* in which two peaks are observed at the binding energy of 529.5 eV and 531.3 eV, which are more than that of 0.2 eV and a third peak is shown at the binding energy of 532.3 eV, which corresponds to the La–O bond and is further confirmed by FTIR analysis. Figure 6e depicted the La 3*d* spectrum of 1.5% La-doped TiO_2. In this figure, the peaks endorsed to the spin split orbit

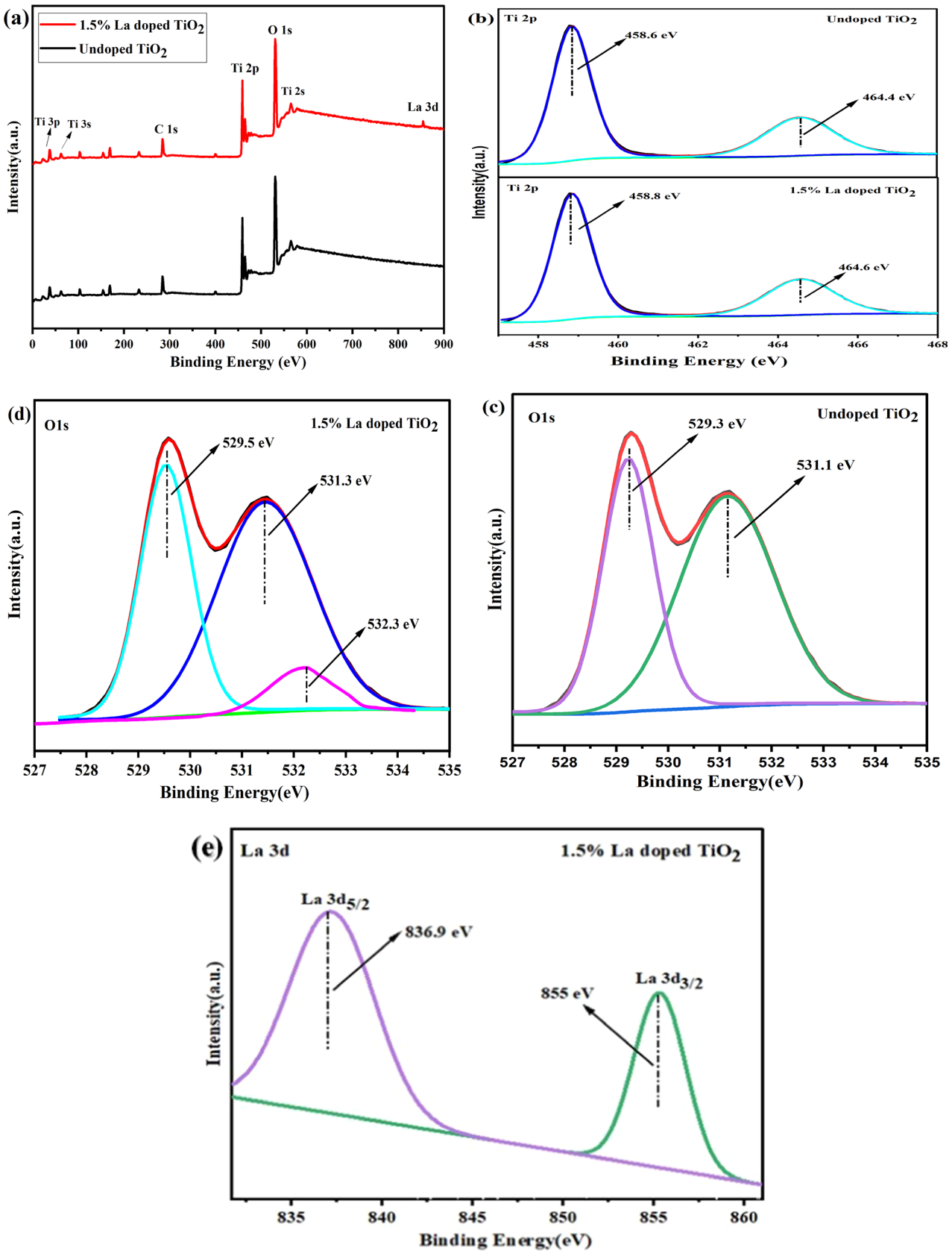

Fig. 6 XPS spectra of **a** total spectra for TiO_2 and 1.5% La-doped TiO_2 **b** fitting curves of the Ti 2*p* regions **c** fitting curve of O 1*s* region of undoped TiO_2 **d** fitting curve of O 1*s* region of 1.5% La-doped TiO_2 **e** fitting curves of La 3*d* regions

La $3d_{3/2}$ and La $3d_{5/2}$ levels, indicating that the presence of La^{3+} species is represented at 853.2 and 836.5 eV, respectively [51, 52]. In the literature, binding energies values of 3*d* shift of La are given as 851.8 eV and 834.9 eV, but here, it is found that these values shift to greater energy levels. This is possible because of the replacement of Ti^{4+} by La^{3+}, so it is clear that there is no incorporation of La in TiO_2's lattice rather than in the configuration of Ti–O–La bond [53–55]. The reason for shifting binding energies in doped TiO_2 is that La is less electronegative than Ti, so charge disparity occurs. As a result, the binding energy alters, and the La electron density in the Ti–O–La decreases [56].

As described earlier in Fig. 6d, the presence of La–O bond can confirm the dopant La has entered the lattices. The oxygen vacancies for charge compensation can be caused by the progress of the acceptor La^{3+} ions into TiO_2 [57] as following:

$$La_2O_3 \rightarrow^{TiO_2} 2La_n' + V_o^{\cdot\cdot} + 3O_o \quad (4)$$

4 Mechanism

Photocatalytic activity of undoped and La-doped TiO_2 nanoparticles was determined by measuring the variation of concentration due to degradation of MB dye solution during photocatalysis in UV-PCR. First, it is well acknowledged that doping with La is likely to develop an oxygen vacancy. The oxygen vacancy may then operate like a trapper to prevent pairs of electrons and holes from recombining, which are photo-generated [58]. Additionally, Wu et al. [59] revealed that when La is doped in TiO_2, it can convert Ti^{4+} to Ti^{3+} via charge compensation. La doping may cause impurity levels due to coaction of Ti^{3+} and oxygen vacancies, which might prevent charge carriers from combining. The other benefit of photocatalytic activity is that La_2O_3 on surface of TiO_2 might move electrons onto the surface. The space charge area gets smaller, and the surface barrier increases as the dopant percentage (La) increases. Additionally, the depth of light penetration into titania significantly surpasses space charge film when the dopant percentage is too prominent. Space charge area becomes quite constrained; as a result, it is simpler to recombine the photogenerated electron–hole pairs [53].

When a photon of appropriate energy is incident on photocatalyst, the electrons are ejected, leaving behind holes. The electrons combine with oxygen to form superoxide. This superoxide radical and holes combine with H_2O to give OH· Radicals [60, 61]. The radicals O_2^{-}· and OH· are highly reactive and oxidise and degrade the organic dyes in the simpler inorganic products [62, 63]. The different equations have been discussed by Raza et al. [64] which shows the production of OH· radical leads to degradation of dye.

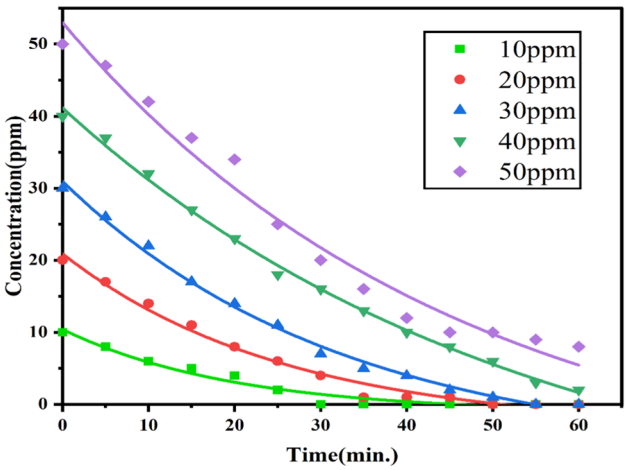

Fig. 7 Effect of residence time on removal of different concentrations of MB by $Ti_{0.985}La_{0.015}O_2$ photocatalyst

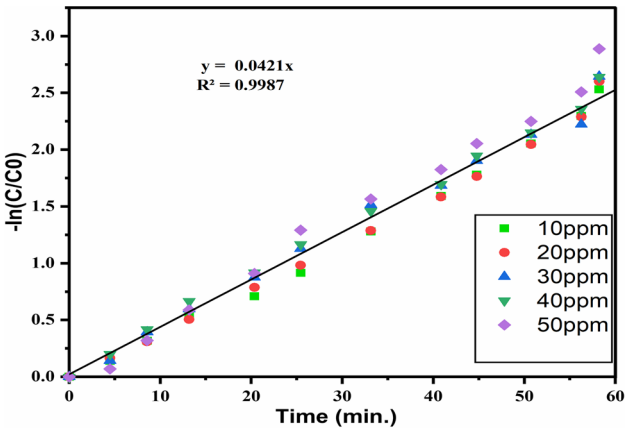

Fig. 8 Kinetic analysis of degradation of MB dye (30 ppm) by Ti0.985La0$_{.015}$O$_2$ photocatalyst, − ln(*C*/Co) versus *t* data

These equations are given below as follows:

$$TiO_2(\text{doped}) + h\nu \rightarrow TiO_2\left(h_{vb}^{+} + e_{cb}^{-}\right) \quad (5)$$

$$O_2^{-} + e_{cb}^{-} \rightarrow O_2^{-\cdot} \quad (6)$$

$$H_2O + h_{vb}^{+} \rightarrow H^{+} + OH^{\cdot} \quad (7)$$

$$OH^{\cdot}/O_2^{-\cdot} + \text{dyes} \rightarrow CO_2 + H_2O \quad (8)$$

4.1 Kinetics Study La-Doped TiO_2

All the catalysts' kinetic analyses were completed, and Figs.7 and 8 depict kinetic data for degradation of MB dye in its

Table 1 Summary of the degree of fitting (R^2) and reaction rate constants of the undoped and La-doped TiO_2 photocatalysts

Catalyst	10 ppm		20 ppm		30 ppm		40 ppm		50 ppm	
	k_p (min^{-1})	R^2	k_p (min^{-1})	R^2	k_p (min^{-1})	R^2	k_p (min^{-1})	R^2	k_p (min^{-1})	R^2
Undoped TiO_2	0.035	0.988	0.036	0.981	0.035	0.973	0.036	0.993	0.039	0.989
$Ti_{0.995}La_{0.005}O_2$	0.041	0.980	0.038	0.971	0.038	0.981	0.037	0.962	0.041	0.995
$Ti_{0.990}La_{0.010}O_2$	0.044	0.981	0.045	0.973	0.041	0.967	0.040	0.995	0.042	0.991
$Ti_{0.985}La_{0.015}O_2$	0.046	0.983	0.046	0.980	0.048	0.995	0.046	0.970	0.047	0.969
$Ti_{0.980}La_{0.020}O_2$	0.045	0.982	0.046	0.986	0.042	0.974	0.045	0.986	0.045	0.982
$Ti_{0.975}La_{0.025}O_2$	0.045	0.981	0.045	0.994	0.039	0.952	0.042	0.989	0.042	0.939

The current results are comparable to various previous literature given in Table 2

aqueous solution with 1.5% La-doped TiO_2 photocatalyst. These figures show the concentration versus time data and the $-\ln(C/Co)$ versus time data, respectively. Pseudo-first-order kinetics Eq. (8) was satisfactorily fitted to kinetic data of degradation of MB dye with all the catalysts as evidenced high R^2 values.

$$-dC/dt = k_p C \tag{9}$$

From the graph of $-\ln(C/Co)$ versus time, the k_p values were determined and shown in Table 1 along with R^2 values. Compared to undoped TiO_2, the catalysts' reaction rate has increased significantly by doping with lanthanum. TiO_2 doped with 1.5% La has the maximum reaction rate constant, which is consistent with other results [51].

It is impressive that the rate of MB's photocatalytic degradation first rises with an increased doping percentage of La before showing a reversal pattern after the amount of La reaches its optimum level. The space charger zone became small, which helped photogenerated pairs of electrons and holes separate effectively. As the percentage of La surged, specialized surface area expanded, and obstructions to the surface improved. The space charge area becomes extremely small when the percentage of La is very high, which might enable light to penetrate titania much deeper than the space charge layer. As a result, it is simpler to recombine for photogenerated charge carriers, and the photocatalytic activity would be decreased [55].

According to an adsorption investigation of the dye on the nanoparticles, only 1–2% of the dye was retained on the photocatalyst's surface. A negligible amount of the dye was photodegraded when no photocatalysts were present in the UV light source.

The reusability of photocatalysts is vital for industrial applications and economy. Figure 9 shows the results of the successive reusability experiments with best photocatalyst (1.5% La-doped TiO_2) performed for five cycles. Figure 9 reveals that degradation in 40 min continuously decreases (85.72–77.87%) from first to fifth cycle, however, with fresh catalyst degradation was 88.71%. So, there is a very small reduction in degradation efficiency (7.85%) after fifth cycle. It is also evident from Fig. 9 that the shape of all the curves is almost similar. The above analysis concludes that 1.5% La-doped TiO_2 is highly stable throughout the photocatalytic degradation of MB dye.

Figure 10 displays the pictographic representation of photocatalytic breakdown of the MB dye of 30 ppm with 0.01 g of photocatalyst $Ti_{0.985}La_{0.015}O_2$ in UV-PCR at the time interval of 5 min. Here, in this sample 1, 2, 3,…, 10 represents MB concentration after time at 0, 5, 10,…, 45 min, respectively.

Aeroxide P-25 and the best-doped TiO_2 sample, $Ti_{0.985}La_{0.015}O_2$, as well as the prepared undoped TiO_2 were compared; the results are given in Fig. 11. The results show that the TiO_2 doped with 1.5% La ($Ti_{0.985}La_{0.015}O_2$) displayed the best photocatalytic performance.

The doping of La could reduce the band gap hence providing a potential to use more part of solar spectrum for degradation of pollutants, and also, it can be used in solar cells for future research.

5 Conclusion

TiO_2 and La-doped [$LaTi_{1-x}La_xO_2$ (x = 0.00–0.025)] nanoparticles could be prepared by solution-combustion process. The prepared nanoparticles were characterized by XRD, FTIR, FE-SEM, DRS and XPS. Photocatalytic performance of each prepared bare and doped TiO_2 photocatalyst was assessed using UV-PCR. The kinetic investigations of all catalysts show that 1.5% La-doped TiO_2 nanoparticles have the best activity for the photocatalysis process in the UV-PCR reactor midst all the synthesized photocatalysts. The current study also discovered that as soon as the La concentration rises to 1.5%, so does activity of TiO_2 to photodegradation; however, the photocatalytic activity begins to diminish after doping concentration increases beyond 1.5%. At 1.5% La doping, TiO_2 had the maximum photocatalytic activity. The

Table 2 Comparison of photocatalytic activity of various photocatalysts with different pollutants

Catalyst	Optimum doping	Pollutant	Light source	Time (min)	Degradation efficiency (%)	Ref
Sn-doped TiO_2	5% mol	MB	125 W Hg lamp	120	77	[65]
Ag-doped TiO_2	0.5% mol	Methyl orange	500 W Xe lamp	180	52.1	[66]
Gd-doped TiO_2	0.3% mol	Methyl orange	500 W Hg lamp	28	50	[67]
Fe-doped TiO_2	1.5% mol	2,4 D	Mercury lamp of 15 watts	120	65	[68]
Fe–N co-doped TiO_2	1% Fe and % N mol	MB	25 W fluorescent lamp	300	80.5	[69]
La–V co-doped TiO_2	10% V and 5% La mol	Methyl orange	Xenon lamp reactor 500 W	180	70	[70]
La-doped TiO_2	1.5% mol	MB	UV photochemical reactor with 8W 8 tubes	40	88.71	Present work

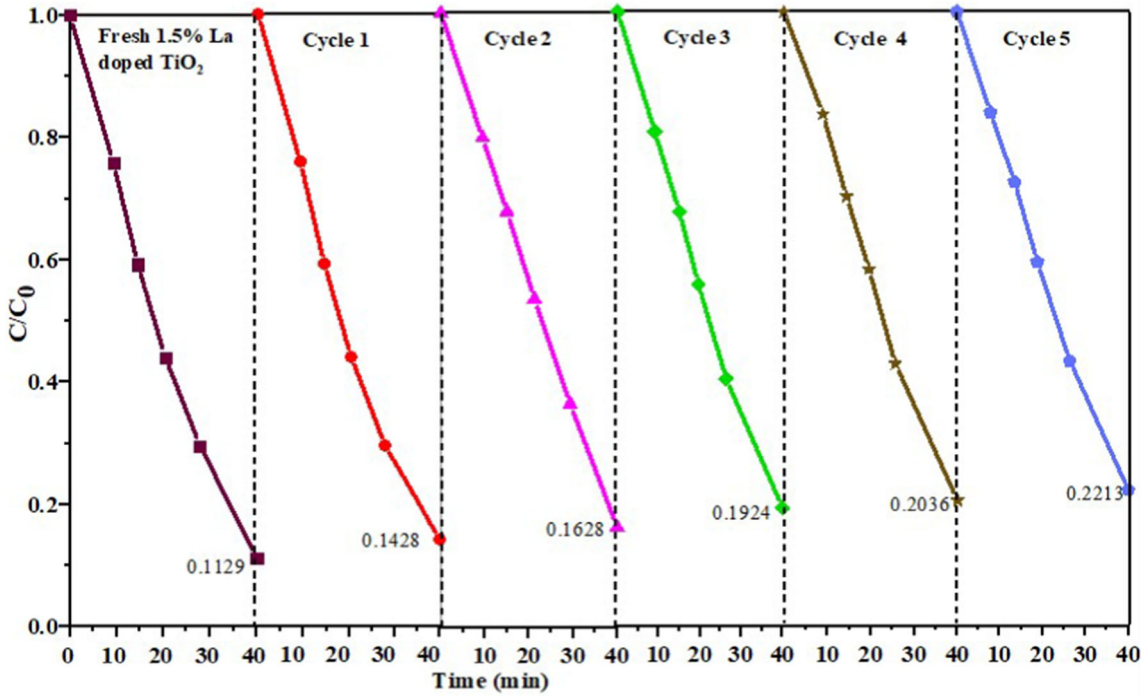

Fig. 9 The reusability of 1.5% La-doped TiO_2 for the breakdown of MB dye at 30 ppm

results of a comparative investigation between synthesized undoped TiO_2, 1.5% La-doped TiO_2, and Aeroxide P-25 photocatalysts demonstrate that the synthesized 1.5% La-doped TiO_2 photocatalyst outperforms the undoped TiO_2 and P-25 photocatalysts. The utilized photocatalyst ($Ti_{0.985}La_{0.015}O_2$) was reused after regeneration for five times to degrade MB dye; the reuse makes photodegradation process more economical. The results of the photodegradation indicate that the $Ti_{0.985}La_{0.015}O_2$ photocatalyst's performance diminishes with the number of reuses.

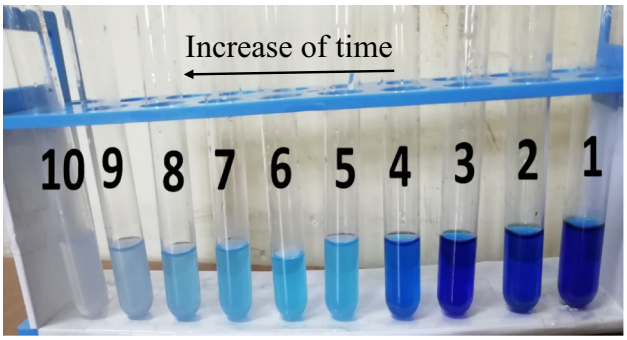

Fig. 10 Pictographic depiction of degradation of MB dye of initial concentration 30 ppm in aqueous solution in UV-PCR reactor using 0.01 g $Ti_{0.985}La_{0.015}O_2$ photocatalyst

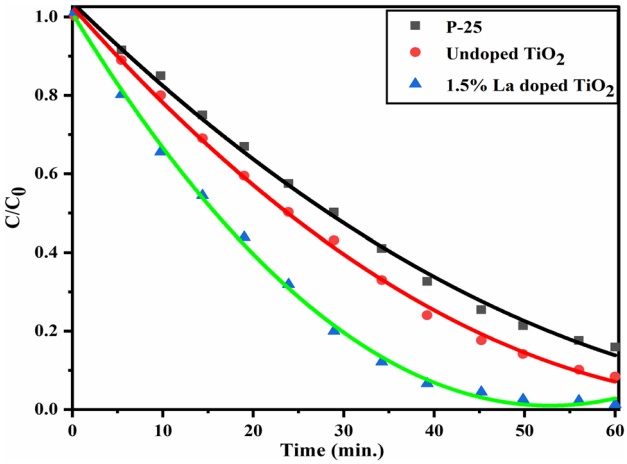

Fig. 11 Comparison of the best photocatalyst among undoped TiO_2, $Ti_{0.985}La_{0.015}O_2$ and aeroxide P-25 for degradation of the MB dye of initial concentration 30 ppm

Supplementary Information The online version contains supplementary material available at https://doi.org/10.1007/s13369-023-08325-3.

Acknowledgements No external grant was received.

Funding The authors declare that no funds, grants, or other support were received during the preparation of this manuscript.

Declarations

Conflict of interest The authors have no relevant financial or non-financial interests to disclose.

References

1. Rasalingam, S.; Peng, R.; Koodali, R.T.: An insight into the adsorption and photocatalytic degradation of rhodamine B in periodic mesoporous materials. Appl. Catal. B Environ. **174–175**, 49–59 (2015). https://doi.org/10.1016/j.apcatb.2015.02.040
2. Bhatti, H.N.; Akhtar, N.; Saleem, N.: Adsorptive removal of methylene blue by low-cost citrus sinensis bagasse: equilibrium, kinetic and thermodynamic characterization. Arab. J. Sci. Eng. **37**, 9–18 (2012). https://doi.org/10.1007/s13369-011-0158-1
3. Li, H.; Budarin, V.L.; Clark, J.H.; North, M.; Wu, X.: Rapid and efficient adsorption of methylene blue dye from aqueous solution by hierarchically porous, activated starbons®: mechanism and porosity dependence. J. Hazard. Mater. **436**, 129174 (2022). https://doi.org/10.1016/j.jhazmat.2022.129174
4. Gautam, A.; Kumar Mondal, M.: Post-combustion capture of CO_2 using novel aqueous triethylenetetramine and 2-dimethylaminoethanol amine blend: equilibrium CO_2 loading-empirical model and optimization, CO_2 desorption, absorption heat, and 13C NMR analysis. Fuel **331**, 125864 (2023). https://doi.org/10.1016/j.fuel.2022.125864
5. Arslan, I.; Balcioglu, I.A.: Degradation of commercial reactive dyestuffs by heterogenous and homogenous advanced oxidation processes: a comparative study. Dye. Pigment. **43**, 95–108 (1999). https://doi.org/10.1016/S0143-7208(99)00048-0
6. Aboua, K.N.; Yobouet, Y.A.; Yao, K.B.; Goné, D.L.; Trokourey, A.: Investigation of dye adsorption onto activated carbon from the shells of Macoré fruit. J. Environ. Manag. **156**, 10–14 (2015). https://doi.org/10.1016/j.jenvman.2015.03.006
7. Bouazizi, A.; Breida, M.; Achiou, B.; Ouammou, M.; Calvo, J.I.; Aaddane, A.; Younssi, S.A.: Removal of dyes by a new nano–TiO_2 ultrafiltration membrane deposited on low-cost support prepared from natural Moroccan bentonite. Appl. Clay Sci. **149**, 127–135 (2017). https://doi.org/10.1016/j.clay.2017.08.019
8. Sahinkaya, E.; Sahin, A.; Yurtsever, A.; Kitis, M.: Concentrate minimization and water recovery enhancement using pellet precipitator in a reverse osmosis process treating textile wastewater. J. Environ. Manag. **222**, 420–427 (2018). https://doi.org/10.1016/j.jenvman.2018.05.057
9. Galindo, C.; Jacques, P.; Kalt, A.: Photooxidation of the phenylazonaphthol AO20 on TiO_2: Kinetic and mechanistic investigations. Chemosphere **45**, 997–1005 (2001). https://doi.org/10.1016/S0045-6535(01)00118-7
10. Gupta, A.; Khosla, N.; Govindasamy, V.; Saini, A.; Annapurna, K.; Dhakate, S.R.: Trimetallic composite nanofibers for antibacterial and photocatalytic dye degradation of mixed dye water. Appl. Nanosci. **10**, 4191–4205 (2020). https://doi.org/10.1007/s13204-020-01540-6
11. Kumari, P.; Kumar, A.: Advanced oxidation process: a remediation technique for organic and non-biodegradable pollutant. Results Surf. Interfaces **11**, 100122 (2023). https://doi.org/10.1016/j.rsurfi.2023.100122
12. Davarnejad, R.; Vasheghani Farahani, J.; Azizi, J.: Petrochemical alcoholic wastewater treatment using an advanced oxidation process: an intensified process for treating an industrial wastewater. Arab. J. Sci. Eng. **48**, 9159–9169 (2023). https://doi.org/10.1007/s13369-022-07164-y
13. Saravanan, A.; Deivayanai, V.C.; Kumar, P.S.; Rangasamy, G.; Hemavathy, R.V.; Harshana, T.; Gayathri, N.; Alagumalai, K.: A detailed review on advanced oxidation process in treatment of wastewater: mechanism, challenges and future outlook. Chemosphere **308**, 136524 (2022). https://doi.org/10.1016/j.chemosphere.2022.136524
14. Chen, C.; Zhao, W.; Li, J.; Zhao, J.; Hidaka, H.; Serpone, N.: Formation and identification of intermediates in the visible-light-assisted photodegradation of sulforhodamine-B dye in aqueous TiO_2 dispersion. Environ. Sci. Technol. **36**, 3604–3611 (2002). https://doi.org/10.1021/es0205434
15. Wang, J.; Li, J.; Xie, Y.; Li, C.; Han, G.; Zhang, L.; Xu, R.; Zhang, X.: Investigation on solar photocatalytic degradation of various

dyes in the presence of Er^{3+}:$YAlO_3$/ZnO–TiO_2 composite. J. Environ. Manag. **91**, 677–684 (2010). https://doi.org/10.1016/j.jenvman.2009.09.031
16. Wang, F.; Xu, M.; Wei, L.; Wei, Y.; Hu, Y.; Fang, W.; Zhu, C.G.: Fabrication of La-doped TiO_2 film electrode and investigation of its electrocatalytic activity for furfural reduction. Electrochim. Acta **153**, 170–174 (2015). https://doi.org/10.1016/j.electacta.2014.11.203
17. Shi, H.; Zhang, T.; Wang, H.: Preparation and photocatalytic activity of La^{3+} and Eu^{3+} co-doped TiO_2 nanoparticles: photo-assisted degradation of methylene blue. J. Rare Earths **29**, 746–752 (2011). https://doi.org/10.1016/S1002-0721(10)60535-2
18. Zhou, J.; Takeuchi, M.; Ray, A.K.; Anpo, M.; Zhao, X.S.: Enhancement of photocatalytic activity of P25 TiO_2 by vanadium-ion implantation under visible light irradiation. J. Colloid Interface Sci. **311**, 497–501 (2007). https://doi.org/10.1016/j.jcis.2007.03.007
19. Zhang, Y.; Zhang, H.; Xu, Y.; Wang, Y.: Europium doped nanocrystalline titanium dioxide: preparation, phase transformation and photocatalytic properties. J. Mater. Chem. **13**, 2261–2265 (2003). https://doi.org/10.1039/b305538h
20. Koepke, C.; Wisniewski, K.; Sikorski, L.; Piatkowski, D.; Kowalska, K.; Naftaly, M.: Upconverted luminescence under 800 nm laser diode excitation in Nd^{3+}-activated fluoroaluminate glass. Opt. Mater. (Amst) **28**, 129–136 (2006). https://doi.org/10.1016/j.optmat.2004.10.034
21. Zhu, J.; Zhu, K.; Chen, L.: Influence of gold nanoparticles on the up-conversion fluorescence in Sm^{3+}. J. Non Cryst. Solids **352**, 150–154 (2006). https://doi.org/10.1016/j.jnoncrysol.2005.11.010
22. Ranjit, K.T.; Willner, I.; Bossmann, S.H.; Braun, A.M.: Lanthanide oxide-doped titanium dioxide photocatalysts: novel photocatalysts for the enhanced degradation of p-chlorophenoxyacetic acid. Environ. Sci. Technol. **35**, 1544–1549 (2001). https://doi.org/10.1021/es001613e
23. Gâcon, J.C.; Horchani, K.; Jouini, A.; Dujardin, C.; Kamenskikh, I.: Optical properties of praseodymium concentrated phosphates. Opt. Mater. (Amst) **28**, 14–20 (2006). https://doi.org/10.1016/j.optmat.2004.10.027
24. Linsebigler, A.L.; Lu, G.; Yates, J.T.: Photocatalysis on TiO_2 surfaces: principles, mechanisms, and selected results. Chem. Rev. **95**, 735–758 (1995). https://doi.org/10.1021/cr00035a013
25. Serpone, N.; Sauvé, G.; Koch, R.; Tahiri, H.; Pichat, P.; Piccinini, P.; Pelizzetti, E.; Hidaka, H.: Standardization protocol of process efficiencies and activation parameters in heterogeneous photocatalysis: relative photonic efficiencies ζr. J. Photochem. Photobiol. A Chem. **94**, 191–203 (1996). https://doi.org/10.1016/1010-6030(95)04223-7
26. Habibi, M.H.; Habibi, A.H.; Zendehdel, M.; Habibi, M.: Dye-sensitized solar cell characteristics of nanocomposite zinc ferrite working electrode: effect of composite precursors and titania as a blocking layer on photovoltaic performance. Spectrochim. Acta Part A Mol. Biomol. Spectrosc. **110**, 226–232 (2013). https://doi.org/10.1016/j.saa.2013.03.051
27. Saroj, S.; Singh, L.; Ranjan, R.; Singh, S.V.: Enhancement of photocatalytic activity and regeneration of Fe-doped TiO_2 ($Ti_{1-x}Fe_xO_2$) nanocrystalline particles synthesized using inexpensive TiO_2 precursor. Res. Chem. Intermed. **45**, 1883–1906 (2019). https://doi.org/10.1007/s11164-018-3708-2
28. Choi, J.; Park, H.; Hoffmann, M.R.: Effects of single metal-ion doping on the visible-light photoreactivity of TiO_2. J. Phys. Chem. C **114**, 783–792 (2010). https://doi.org/10.1021/jp908088x
29. Tab, A.; Dahmane, M.; Belabed, C.; Bellal, B.; Richard, C.; Trari, M.: High efficiency photocatalytic degradation of ambroxol over Mn doped TiO_2: experimental designs, identification of transformation products, mineralization and mechanism. Sci. Total. Environ. (2021). https://doi.org/10.1016/j.scitotenv.2021.146451
30. Wang, Q.; Rhimi, B.; Wang, H.; Wang, C.: Efficient photocatalytic degradation of gaseous toluene over F-doped TiO_2/exfoliated bentonite. Appl. Surf. Sci. **530**, 1–12 (2020). https://doi.org/10.1016/j.apsusc.2020.147286
31. Basavarajappa, P.S.; Patil, S.B.; Ganganagappa, N.; Reddy, K.R.; Raghu, A.V.; Reddy, C.V.: Recent progress in metal-doped TiO_2, non-metal doped/codoped TiO_2 and TiO_2 nanostructured hybrids for enhanced photocatalysis. Int. J. Hydrog. Energy **45**, 7764–7778 (2020). https://doi.org/10.1016/j.ijhydene.2019.07.241
32. Barkul, R.P.; Sutar, R.S.; Patil, M.K.; Delekar, S.D.: Photocatalytic degradation of organic pollutants by using nanocrystalline boron-doped TiO_2 catalysts. Chem. Sel. **6**, 3360–3369 (2021). https://doi.org/10.1002/slct.202003910
33. Saroj, S.; Singh, L.; Singh, S.V.: Solution-combustion synthesis of anion (iodine) doped TiO_2 nanoparticles for photocatalytic degradation of Direct Blue 199 dye and regeneration of used photocatalyst. J. Photochem. Photobiol. A Chem. **396**, 112532 (2020). https://doi.org/10.1016/j.jphotochem.2020.112532
34. Kayani, Z.N.; Rahim, S.; Sagheer, R.; Riaz, S.; Naseem, S.: Assessment of antibacterial and optical features of sol-gel dip coated La doped TiO_2 thin films. Mater. Chem. Phys. **250**, 123217 (2020). https://doi.org/10.1016/j.matchemphys.2020.123217
35. Kayani, Z.N.; Maria; Riaz, S.; Naseem, S.: Magnetic and antibacterial studies of sol–gel dip coated Ce doped TiO_2 thin films: influence of Ce contents. Ceram. Int. **46**, 381–390 (2020). https://doi.org/10.1016/j.ceramint.2019.08.272
36. Madhvi; Singh, L.; Saroj, S.; Lee, Y.; Singh, S.V.: Facile synthesis of nano-crystalline anatase TiO_2 and their applications in degradation of direct blue 199. J. Mater. Sci. Mater. Electron. **27**, 2581–2588 (2016). https://doi.org/10.1007/s10854-015-4061-5
37. Saroj, S.; Singh, L.; Singh, S.V.: Photodegradation of direct blue-199 in carpet industry wastewater using iron-doped TiO_2 nanoparticles and regenerated photocatalyst. Int. J. Chem. Kinet. **51**, 189–205 (2019). https://doi.org/10.1002/kin.21243
38. Shi, Z.; Zhang, X.; Yao, S.: Preparation and photocatalytic activity of TiO_2 nanoparticles co-doped with Fe and la. Particuology. **9**, 260–264 (2011). https://doi.org/10.1016/j.partic.2010.05.017
39. Pascariu, P.; Cojocaru, C.; Homocianu, M.; Samoila, P.; Dascalu, A.; Suchea, M.: New La^{3+} doped TiO_2 nanofibers for photocatalytic degradation of organic pollutants: effects of thermal treatment and doping loadings. Ceram. Int. **48**, 4953–4964 (2022). https://doi.org/10.1016/j.ceramint.2021.11.033
40. Kamble, R.J.; Gaikwad, P.V.; Garadkar, K.M.; Sabale, S.R.; Puri, V.R.; Mahajan, S.S.: Photocatalytic degradation of malachite green using hydrothermally synthesized cobalt-doped TiO_2 nanoparticles. J. Iran. Chem. Soc. **19**, 303–312 (2022). https://doi.org/10.1007/s13738-021-02303-y
41. Zhan, C.; Chen, F.; Yang, J.; Dai, D.; Cao, X.; Zhong, M.: Visible light responsive sulfated rare earth doped TiO_2@fumed SiO_2 composites with mesoporosity: enhanced photocatalytic activity for methyl orange degradation. J. Hazard. Mater. **267**, 88–97 (2014). https://doi.org/10.1016/j.jhazmat.2013.12.038
42. Sibu, C.P.; Kumar, S.R.; Mukundan, P.; Warrier, K.G.K.: Structural modifications and associated properties of lanthanum oxide doped sol-gel nanosized titanium oxide. Chem. Mater. **14**, 2876–2881 (2002). https://doi.org/10.1021/cm010966p
43. Nie, J.; Mo, Y.; Zheng, B.; Yuan, H.; Xiao, D.: Electrochemical fabrication of lanthanum-doped TiO_2 nanotube array electrode and investigation of its photoelectrochemical capability. Electrochim. Acta **90**, 589–596 (2013). https://doi.org/10.1016/j.electacta.2012.12.049
44. Coromelci, C.; Ignat, M.; Sacarescu, L.; Neamtu, M.: Enhanced visible light activated mesoporous titania by rare earth metal doping. Microporous Mesoporous Mater. **341**, 112072 (2022). https://doi.org/10.1016/j.micromeso.2022.112072

45. Bashir, A.; Bashir, F.; Sultan, M.; Mubeen, M.; Iqbal, A.; Akhter, Z.: Influence of nickel and lanthanum ions co-doping on photocatalytic properties of TiO_2 for effective degradation of reactive yellow 145 in the visible region. J. Sol Gel Sci. Technol. **93**, 438–451 (2020). https://doi.org/10.1007/s10971-019-05162-5
46. Köseoğlu, Y.: Structural and magnetic properties of Cr doped NiZn-ferrite nanoparticles prepared by surfactant assisted hydrothermal technique. Ceram. Int. **41**, 6417–6423 (2015). https://doi.org/10.1016/j.ceramint.2015.01.079
47. Mathew, D.S.; Juang, R.S.: An overview of the structure and magnetism of spinel ferrite nanoparticles and their synthesis in microemulsions. Chem. Eng. J. **129**, 51–65 (2007). https://doi.org/10.1016/j.cej.2006.11.001
48. Xue, W.; Zhang, G.; Xu, X.; Yang, X.; Liu, C.; Xu, Y.: Preparation of titania nanotubes doped with cerium and their photocatalytic activity for glyphosate. Chem. Eng. J. **167**, 397–402 (2011). https://doi.org/10.1016/j.cej.2011.01.007
49. Yu, L.; Yang, X.; He, J.; He, Y.; Wang, D.: One-step hydrothermal method to prepare nitrogen and lanthanum co-doped TiO_2 nanocrystals with exposed {0 0 1} facets and study on their photocatalytic activities in visible light. J. Alloys Compd. **637**, 308–314 (2015). https://doi.org/10.1016/j.jallcom.2015.03.035
50. Lei, X.F.; Chen, C.; Li, X.; Xue, X.X.; Yang, H.: Characterization and photocatalytic performance of la and C co-doped anatase TiO_2 for photocatalytic reduction of Cr(VI). Sep. Purif. Technol. **161**, 8–15 (2016). https://doi.org/10.1016/j.seppur.2016.01.030
51. Han, M.; Dong, Z.; Liu, J.; Ren, G.; Ling, M.; Yang, X.; Zhang, L.; Xue, B.; Li, F.: The role of lanthanum in improving the visible-light photocatalytic activity of TiO_2 nanoparticles prepared by hydrothermal method. Appl. Phys. A Mater. Sci. Process. **126**, 1–10 (2020). https://doi.org/10.1007/s00339-020-04135-8
52. Parthasarathy, P.; Narayanan, S.K.: Effect of hydrothermal carbonization reaction parameters on. Environ. Prog. Sustain. Energy **33**, 676–680 (2014). https://doi.org/10.1002/ep.11974
53. Cong, Y.; Tian, B.; Zhang, J.: Improving the thermal stability and photocatalytic activity of nanosized titanium dioxide via La^{3+} and N co-doping. Appl. Catal. B Environ. **101**, 376–381 (2011). https://doi.org/10.1016/j.apcatb.2010.10.006
54. Liqiang, J.; Xiaojun, S.; Baifu, X.; Baiqi, W.; Weimin, C.; Honggang, F.: The preparation and characterization of la doped TiO_2 nanoparticles and their photocatalytic activity. J. Solid State Chem. **177**, 3375–3382 (2004). https://doi.org/10.1016/j.jssc.2004.05.064
55. Lan, X.; Wang, L.; Zhang, B.; Tian, B.; Zhang, J.: Preparation of lanthanum and boron co-doped TiO_2 by modified sol-gel method and study their photocatalytic activity. Catal. Today **224**, 163–170 (2014). https://doi.org/10.1016/j.cattod.2013.10.062
56. Yu, L.; Yang, X.; He, J.; He, Y.; Wang, D.: A fluorine free method to synthesize nitrogen and lanthanum co-doped TiO_2 nanocrystals with exposed {0 0 1} facets for enhancing visible-light photocatalytic activity. J. Mol. Catal. A Chem. **399**, 42–47 (2015). https://doi.org/10.1016/j.molcata.2015.01.022
57. Li, J.; Zeng, Y.; Fang, Y.; Chen, N.; Du, G.; Zhang, A.: Synthesis of (La+Nb) co-doped TiO_2 rutile nanoparticles and dielectric properties of their derived ceramics composed of submicron-sized grains. Ceram. Int. **47**, 8859–8867 (2021). https://doi.org/10.1016/j.ceramint.2020.12.007
58. Zhao, N.; Yao, M.M.; Li, F.; Lou, F.P.: Microstructures and photocatalytic properties of Ag and La surface codoped TiO_2 films prepared by solgel method. J. Solid State Chem. **184**, 2770–2775 (2011). https://doi.org/10.1016/j.jssc.2011.08.014
59. Wu, H.H.; Deng, L.X.; Wang, S.R.; Zhu, B.L.; Huang, W.P.; Wu, S.H.; Zhang, S.M.: The preparation and characterization of la doped TiO_2 nanotubes and their photocatalytic activity. J. Dispers. Sci. Technol. **31**, 1311–1316 (2010). https://doi.org/10.1080/01932690903227071
60. Nur, A.S.M.; Sultana, M.; Mondal, A.; Islam, S.; Robel, F.N.; Islam, A.; Sumi, M.S.A.: A review on the development of elemental and codoped TiO_2 photocatalysts for enhanced dye degradation under UV–vis irradiation. J. Water Process Eng. **47**, 102728 (2022). https://doi.org/10.1016/j.jwpe.2022.102728
61. Banu, R.; Salvi, N.; Gupta, S.; Ameta, C.; Ameta, R.; Punjabi, P.B.: A facile Synthesis of GO/CuO nanocomposite with enhancing photocatalytic activity for the degradation of azure-B dye and its antimicrobial behavior. Arab. J. Sci. Eng. **47**, 365–378 (2022). https://doi.org/10.1007/s13369-021-05421-0
62. John Jeya Kamaraj, J.J.; Annamalai, P.; Stephen Tamil, L.D.; Muthu, S.P.; Perumalsamy, R.; Valdes, H.: Enhanced photocatalytic degradation of $ZnTiO_3$/polycarbazole (PCz) composite towards toxic azo dye. Arab. J. Sci. Eng. **48**, 8143–8151 (2023). https://doi.org/10.1007/s13369-022-07570-2
63. Jasim, S.A.; Patra, I.; Abdulhadi, A.M.; Al-Gazally, M.E.; Sharma, H.; Alawsi, T.; Mohammed, H.T.; Hussein, S.A.; Altimari, U.S.; Hammid, A.T.; Chem, C.: Magnetic $CeO_2/SrFe_{12}O_{19}$ nanocomposite: synthesis, characterization and photocatalytic degradation of methyl orange. Arab. J. Sci. Eng. (2022). https://doi.org/10.1007/s13369-022-07044-5
64. Raza, W.; Haque, M.M.; Muneer, M.; Fleisch, M.; Hakki, A.; Bahnemann, D.: Photocatalytic degradation of different chromophoric dyes in aqueous phase using la and Mo doped TiO_2 hybrid carbon spheres. J. Alloys Compd. **632**, 837–844 (2015). https://doi.org/10.1016/j.jallcom.2015.01.222
65. Bayan, E.M.; Lupeiko, T.G.; Pustovaya, L.E.; Volkova, M.G.: Synthesis and photocatalytic properties of Sn–TiO_2 nanomaterials. J. Adv. Dielectr. **10**, 1–10 (2020). https://doi.org/10.1142/S2010135X20600188
66. Nyamukamba, P.; Tichagwa, L.; Mamphweli, S.; Petrik, L.: Silver/carbon Co doped titanium dioxide photocatalyst for improved dye degradation under visible light. Int. J. Photoenergy (2017). https://doi.org/10.1155/2017/3079276
67. Cheng, X.Q.; Ma, C.Y.; Yi, X.Y.; Yuan, F.; Xie, Y.; Hu, J.M.; Hu, B.C.; Zhang, Q.Y.: Structural, morphological, optical and photocatalytic properties of Gd-doped TiO_2 films. Thin Solid Films **615**, 13–18 (2016). https://doi.org/10.1016/j.tsf.2016.06.049
68. Ebrahimi, R.; Maleki, A.; Rezaee, R.; Daraei, H.; Safari, M.; McKay, G.; Lee, S.M.; Jafari, A.: Synthesis and application of Fe-doped TiO_2 nanoparticles for photodegradation of 2,4-D from aqueous solution. Arab. J. Sci. Eng. **46**, 6409–6422 (2021). https://doi.org/10.1007/s13369-020-05071-8
69. Sikirman, A.; Krishnan, J.: Photocatalytic degradation of methylene blue by nanosized visible light active nitrogen and iron Co doped titania: characterization and feasibility investigation. J. Environ. Eng. **142**, 1–8 (2016). https://doi.org/10.1061/(asce)ee.1943-7870.0001028
70. Ilkhechi, N.N.; Ghobadi, N.; Akbarpour, M.R.: Enhanced optical and photo catalytic properties of V and La co doped TiO_2 nanoparticles. J. Mater. Sci. Mater. Electron. **28**, 6426–6434 (2017). https://doi.org/10.1007/s10854-016-6328-x